OPEN ACCESS

University of BRISTOL

Iannelli, A., Marcos, A., & Lowenberg, M. (2017). Nonlinear flutter analysis with uncertainties based on Describing Function and Structured Singular Value with an IQC validation. In *Proceedings of the 7th European Conference for Aeronautics and Space Sciences (EUCASS 20177)* EUCASS Association.

Publisher's PDF, also known as Version of record

Link to publication record on the Bristol Research Portal
PDF-document

This is the final published version of the article (version of record). It first appeared online via http://www.eucass2017.eu for registered attendees only. Please refer to any applicable terms of use of the publisher.

University of Bristol – Bristol Research Portal
General rights

This document is made available in accordance with publisher policies. Please cite only the published version using the reference above. Full terms of use are available:
http://www.bristol.ac.uk/red/research-policy/pure/user-guides/brp-terms/

Nonlinear flutter analysis with uncertainties based on Describing Function and Structured Singular Value with an IQC validation

Andrea Iannelli ⋆†*, Andrés Marcos* ⋆*, Mark Lowenberg* ⋆
⋆*University of Bristol, Department of Aerospace Engineering*
Queen's Building, University Walk, Bristol BS8 1TR, UK
andrea.iannelli · andres.marcos · m.lowenberg@bristol.ac.uk
†Corresponding author

Abstract

This work deals with the stability analysis of an aeroelastic system affected by freeplay and uncertainties. Nonlinearities can trigger Limit Cycle Oscillations (LCOs), self-sustained periodic responses likely to provoke critical damages. Moreover, uncertainties in the models might lead to inaccurate predictions in terms of onset and features of these instabilities. The paper shows a possible strategy to tackle this problem, pivoting on the Describing Functions method to model freeplay and μ analysis to study stability in the face of parametric uncertainties. The simplifying hypotheses underlying the framework are commented, and an approach to validate the main results, by means of Integral Quadratic Constraints, is finally proposed.

1. Introduction

One of the major challenges faced by the aeronautical industry nowadays is to achieve lightweight aircraft configurations which enable to reduce fuel consumptions and operating costs ensuring at the same time a feasible design in terms of safety constraints. Among the most dangerous instability phenomena, exacerbated by wing flexibility, there is flutter.
Flutter is a self-excited instability in which aerodynamic forces acting on a flexible body couple with its structural vibration modes producing oscillatory motion. The level of vibration may result in sufficiently large amplitudes to provoke failure and often this requirement dictates the design of the structure.[12]

Despite the large amount of effort spent in understanding flutter, it is acknowledged that predictions based only on computational analyses are not totally reliable.[19] Currently this is compensated by the addition of conservative safety margins to the analysis results as well as expensive flutter test campaigns. One of the main criticalities arises from the sensitivity of aeroelastic instability to small variations in parameter and modeling assumptions. In addressing this issue, in the last two decades researchers looked at robust modeling and analysis techniques from the robust control community, specifically Linear Fractional Transformation (LFT) models and μ (Structured Singular Value) analysis.[16]

This framework is applicable to the study of robust stability of linear systems, allowing to determine the robust flutter speed (the worst-case flutter speed in the face of the whole set of uncertainties). However, the increase in flexibility on one side and a more realistic description of the system on the other compel to consider cases where the linear hypothesis no longer holds. The aeronautical industry, for example, has recently sensibly strengthen its interest in evaluating the effect of the uncertainties on instabilities prompted by control surface freeplay.[3]
A way to introduce nonlinearities in this context (specifically the so-called hard-nonlinearities) is represented by the Describing Function (DF) method. The main idea is to approximate the nonlinear operator through a linear one which depends on some properties of the input (quasi-linearization). DF has been successfully employed for the prediction of onset, frequency and amplitude of Limit Cycle Oscillations (LCOs) in aeroservoelastic applications.[20] A recent work[14] showed how, in conjunction with μ, DF can be used to inform passive optimal remedies to alleviate the LCO response.

The first contribution of this study is to present a systematic methodology for the application of the DF-μ framework to an aeroelastic system subject to nonlinearities and uncertainties in order to assess the stability and post-critical behaviour. In addition, the stability of the LCO (i.e. whether the predicted oscillations take place or not) can also be studied. While the standard procedure[1] relies on a state-space description of the system, it is proposed in the paper an equivalent formulation for systems described in frequency-domain (as it is the case for flutter analysis in real aeronautical applications[12,13]).

Copyright © 2017 by A. Iannelli, A. Marcos, M. Lowenberg. Published by the EUCASS association with permission.

The prowess of this methodology is showcased by applying it to a benchmark study consisting of a typical section affected by control surface freeplay.[6,20] Nominal analysis is first performed in order to get insight in the system response and properties, showing the usage of both algebraic and graphical methods. The robustness of the LCOs in the face of parametric Linear Time Invariant (LTI) uncertainties is then assessed.

In order to apply this approach for the analysis of nonlinear and uncertain systems, simplifying hypotheses must be made. For example, the key assumption of DF consists in assuming that the linear part of the system filters out the higher harmonics in the output of the nonlinearity (such that it outputs a pure sinusoid). Although previous studies applied to this benchmark proved its applicability,[17,20] this assumption is highly case-dependent and it is envisaged the need to provide a general validation framework for the results obtained with this approach.
Prompted by these considerations, Integral Quadratic Constraints (IQCs) are employed. IQCs are a tool giving sufficient conditions for the stability of uncertain nonlinear systems.[18] Some of the results obtained with the robust quasi-linear analysis are revisited within this more comprehensive framework, pointing out a possible two-step approach to deal with nonlinear robust problems.

The layout of the article is as follows. Section 2 gives an overview for each one of the techniques employed in the work, whereas Section 3 introduces the aeroelastic model. Section 4 describes the methodology to detect LCOs and study their stability, and finally Section 5 presents and comments the results of the analyses.

2. Theoretical background

This Section presents the necessary theoretical background by means of a cursory introduction to the techniques employed in the work. As concerns the notation, common definitions are adopted.[11,18,23]

2.1 Describing Functions

The analysis and design of linear plants pivots on a complex-valued function, the frequency response. However, this function cannot be defined for nonlinear systems, hence frequency-domain techniques cannot be directly applied. The Describing Function (DF) method[11] aims to overcome this obstacle by providing in these cases an alternative definition of frequency response.

The DF method is mostly applied to systems which can be recast in the framework of Fig. 1, characterised by having separable linear and nonlinear parts connected in a single loop configuration. An example is provided by *hard nonlinearities* (e.g. saturation, freeplay, hysteresis), which are nonlinearities characterized by discontinuities and thus cannot be locally approximated by linear functions.

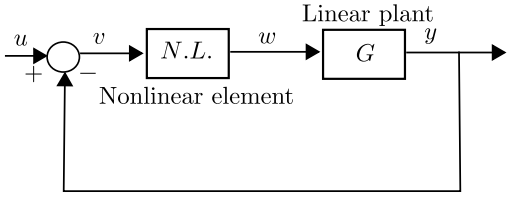

Figure 1: Feedback representation of a nonlinear system

The concept of *quasi-linearization* is the basis of the application of DF. This is aimed at retaining the advantages of a linear approximation without the constraint of requiring small departures of the variables from the nominal operating values and it can be achieved if the approximation of the nonlinear operator depends on some properties of the input. By using quasi-linearization the dependence of performance on signal amplitude, the basic characteristic of nonlinear behavior, is thus retained.
The quasi-linearization process requires that the input signal *form* is specified. In analogy to what is done in frequency-domain analysis, it is widely employed the concept of a sinusoidal-input describing function (SIDF), in the following simply abbreviated as DF. The interest in periodic signals is mainly dictated by the aim to detect and analyse steady oscillations in nonlinear systems, also known as Limit Cycle Oscillations (LCOs).

Consider a sinusoidal signal $v(t)$ of amplitude A and frequency ω at the nonlinear element. If the nonlinearity is single-valued (i.e. only one output is possible for any given value of the input, also called memoryless), the output w(t) is a periodic function and thus can be expanded using Fourier series:

$$w(t) = \frac{a_0}{2} + \sum_{n=1}^{\infty} [a_n(A,\omega)\cos(n\omega t) + b_n(A,\omega)\sin(n\omega t)] \tag{1}$$

where a_n and b_n are the Fourier coefficients obtained by integration and are function of A and ω. If an odd nonlinearity (i.e. the relation between the input and output of the nonlinear block is symmetric about the origin) is considered, then a_0=0. This assumption is introduced to further simplify Eq. (1), without loss of generality.
The *key* hypothesis of the DF method is that only the fundamental component has to be retained from the generical periodic output $w(t)$. This is an approximation because the output of a nonlinear element corresponding to a sinusoidal input usually contains higher harmonics. The rationale underpinning this assumption is that the higher harmonics in the output are filtered out, i.e. the linear element satisfies the low-pass filter condition (or *filter hypothesis*):

$$\|G(j\omega)\| \gg \|G(jn\omega)\| \quad \text{for} \quad n = 2, 3, ... \tag{2}$$

The DF of a nonlinear element is thus the complex fundamental-harmonic gain of a nonlinearity in the presence of a driving sinusoid of amplitude A:

$$\begin{aligned} N(A,\omega) &= \frac{Me^{j(\omega t+\theta)}}{Ae^{j(\omega t)}} = \frac{M}{A}e^{j\theta} = \frac{b_1 + ja_1}{A} \\ \text{with} \quad M(A,\omega) &= \sqrt{a_1^2 + b_1^2}; \quad \theta(A,\omega) = \arctan\left(\frac{a_1}{b_1}\right) \end{aligned} \tag{3}$$

This method hence consists in treating the nonlinear element of Fig. 1 in the presence of a sinusoidal input as if it were a linear element with a frequency response $N(A, \omega)$.

The main hypotheses connected with the application of the DF method are:

- The nonlinear element is time-invariant
- The actual signal at the nonlinearity input has a form resembling the one used to derive the describing function
- The output of the nonlinear element in response to a sinusoid is periodic (always true when the nonlinearity is single-valued)
- The linear part of the system acts as a low pass filter, i.e. condition in Eq. (2) is satisfied

2.2 LFT modeling and μ analysis

LFT is an instrumental framework in modern control theory for robustness analysis and synthesis. The underpinning idea is to represent an uncertain systems in terms of nominal and uncertain components given by matrices.
If the *coefficient matrix* $\mathbf{M}$ is defined as a proper transfer matrix, $\mathcal{F}_u$, namely the upper LFT,[23] is the closed-loop transfer matrix from input $\mathbf{u}$ to output $\mathbf{y}$ when the nominal plant $\mathbf{M_{22}}$ is subject to a perturbation matrix $\mathbf{\Delta_u}$ (Fig. 2).

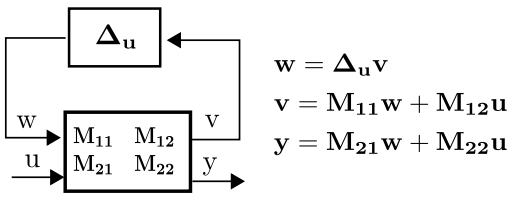

Figure 2: Upper LFT

$\mathbf{M_{11}}$,$\mathbf{M_{12}}$ and $\mathbf{M_{21}}$ reflect a priori knowledge of how the perturbation affects the system. The algebraic expression for $\mathcal{F}_u$ is given by:

$$\mathcal{F}_u(\mathbf{M}, \mathbf{\Delta_u}) = \mathbf{M_{22}} + \mathbf{M_{21}}\mathbf{\Delta_u}(\mathbf{I} - \mathbf{M_{11}}\mathbf{\Delta_u})^{-1}\mathbf{M_{12}} \tag{4}$$

This LFT is well posed if and only if the inverse of $(\mathbf{I} - \mathbf{M_{11}}\mathbf{\Delta_u})$ exists.

μ analysis enables the robust stability and performance of a system subject to real parametric and dynamic uncertainties to be addressed.
The structured singular (s.s.v.) value of a matrix $\mathbf{M} \in C^{n\times n}$ is denoted by $\mu_{\mathbf{\Delta}}(\mathbf{M})$, where $\mathbf{\Delta}$ is a structured uncertainty set.[2] The mathematical definition follows:

$$\mu_{\mathbf{\Delta}}(\mathbf{M}) = \left(\min_{\hat{\mathbf{\Delta}}\in\mathbf{\Delta}} (\bar{\sigma}(\hat{\mathbf{\Delta}}) : \det\left(\mathbf{I} - \mathbf{M}\hat{\mathbf{\Delta}}\right) = 0)\right)^{-1} \tag{5}$$

if $\exists\hat{\mathbf{\Delta}} \in \mathbf{\Delta}$ such that $\det\left(\mathbf{I} - \mathbf{M}\hat{\mathbf{\Delta}}\right) = 0$ and otherwise $\mu_{\mathbf{\Delta}}(\mathbf{M}) := 0$, and $\bar{\sigma}(\hat{\mathbf{\Delta}})$ is the maximum singular value of $\hat{\mathbf{\Delta}}$.
Note that this definition can be specialized to determine whether the LFT $\mathcal{F}_u(\mathbf{M}, \mathbf{\Delta_u})$ is well posed once the generic matrix $\mathbf{M}$ in the above definition is replaced by $\mathbf{M_{11}}$ and $\mathbf{\Delta}$ coincides with the corresponding uncertainty set $\mathbf{\Delta_u}$. The robust stability (RS) problem can then be formulated as a μ calculation:

$$\mu_{\mathbf{\Delta_u}}(\mathbf{M_{11}}) = \left(\min_{\hat{\mathbf{\Delta}}\in\mathbf{\Delta_u}}\left(\hat{\beta} : \det\left(\mathbf{I} - \hat{\beta}\mathbf{M_{11}}\hat{\mathbf{\Delta}}\right) = 0; \quad \bar{\sigma}(\hat{\mathbf{\Delta}}) \leq 1\right)\right)^{-1} \tag{6}$$

where $\hat{\beta}$ is a real positive scalar. For ease of calculation and interpretation, this set is norm-bounded (i.e. $\bar{\sigma}(\mathbf{\Delta_u}) < 1$) by scaling of $\mathbf{M_{11}}$. The result can then be interpreted as follows: if $\mu_{\mathbf{\Delta_u}}(\mathbf{M_{11}}) \leq 1$ then there is no perturbation matrix inside the allowable set $\mathbf{\Delta_u}$ such that the determinant condition is satisfied, that is, the associated plant is robustly stable. On the contrary, if $\mu_{\mathbf{\Delta_u}}(\mathbf{M_{11}}) \geq 1$ a candidate (i.e. belonging to the allowed set) perturbation matrix exists which violates the well-posedness.

Finally, it is worth highlighting that $\mu_{\mathbf{\Delta}}(\mathbf{M})$ is in general an NP-hard problem, thus all μ algorithms work by searching for upper and lower bounds. In this work, the routines available in the Robust Control Toolbox (RCT) in MATLAB[2] are employed.

2.3 Integral Quadratic Constraints

IQC is a well established technique to deal with stability and performance analysis of nonlinear and uncertain systems[18] in a unified framework. Let us consider the problem in Fig. 3, where G is an LTI system and Δ is here generically a casual and bounded operator. $\mathcal{L}_2^n[0,\infty]$ will denote the vector space of all square integrable functions.

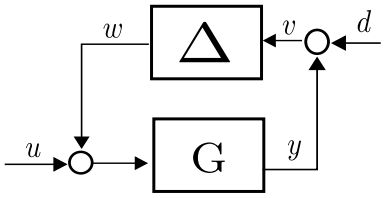

Figure 3: Feedback interconnection

The basic idea is to describe the nonlinear uncertain operator $\Delta : \mathcal{L}_2^n[0,\infty] \to \mathcal{L}_2^m[0,\infty]$ by means of an integral quadratic constraint on its input and output channels. Let $\Pi : j\mathbb{R} \to \mathbb{C}^{(n+m)\times(n+m)}$ be a measurable Hermitian-valued function (usually chosen among the rational functions bounded on the imaginary axis), commonly named multiplier. Two signals $v \in \mathcal{L}_2^n[0,\infty]$ and $w \in \mathcal{L}_2^m[0,\infty]$ satisfy the IQC defined by Π if:

$$\int_{-\infty}^{+\infty} \begin{bmatrix}\hat{v}(j\omega)\\ \hat{w}(j\omega)\end{bmatrix}^* \Pi(j\omega) \begin{bmatrix}\hat{v}(j\omega)\\ \hat{w}(j\omega)\end{bmatrix} d\omega \geq 0 \tag{7}$$

A bounded and casual operator Δ is said to satisfy the IQC defined by Π if the signals v and $w = \Delta(v)$ satisfy Eq. (7) for all v. The next theorem provides a stability condition for the interconnection of G and Δ.

Theorem 1 *Let $G \in \mathbb{RH}_\infty$ and Δ be a casual bounded operator. Assume for all $\tau \in [0,1]$:*

1. *the interconnection of G and $\tau\Delta$ is well-posed.*
2. *$\tau\Delta$ satisfies the IQC defined by Π.*
3. *$\exists\, \epsilon$ such that*

$$\begin{bmatrix}G(j\omega)\\ I\end{bmatrix}^* \Pi(j\omega) \begin{bmatrix}G(j\omega)\\ I\end{bmatrix} d\omega \leq -\epsilon I \quad \forall\omega \in \mathbb{R} \tag{8}$$

Then the feedback interconnection of G and Δ is stable.[18]

In order to facilitate the numerical solution of this problem, it is common practice to parameterize the multiplier Π. In case $\Pi \in \mathbb{RL}_\infty^{(n+m)\times(n+m)}$, this can be factorized as $\Pi = \Psi^{\sim}\, S\, \Psi$ where $S = S^T$ is a real matrix variable and $\Psi \in \mathbb{RH}_\infty^{(n+m)\times(n+m)}$ is constructed from pre-selected basis transfer functions. This factorization allows therefore to

separate the dynamic part from the decision variables.
The Condition 3 in Theorem 1 can then be equivalently rewritten as:

$$\Phi(j\omega)^* S\,\Phi(j\omega) < 0 \quad \forall\omega \in \mathbb{R} \tag{9}$$

with:

$$\Phi(j\omega) = \Psi(j\omega)\begin{bmatrix} G(j\omega) \\ I \end{bmatrix} = \check{C}(j\omega - \check{A})^{-1}\check{B} + \check{D} \tag{10}$$

The next fundamental theorem can hence be recalled.

Theorem 2 *The KYP Lemma[18] states that Eq. (9) holds true if and only if there exists a matrix $P = P^T$ such that:*

$$\begin{bmatrix} \check{A}^T P + P\check{A} & P\check{B} \\ \check{B}^T P & 0 \end{bmatrix} + \begin{bmatrix} \check{C}^T \\ \check{D}^T \end{bmatrix} S \begin{bmatrix} \check{C} & \check{D} \end{bmatrix} < 0 \tag{11}$$

This result enables to connect the stability of the interconnection G–Δ in Fig. 3 with the solution of the Linear Matrix Inequality (LMI) problem in Eq. (11) and represents the standard way to solve IQC problems.

Theorem 2 allows to transform the infinite set of constraints in Eq. (9) into the single constraint in Eq. (11) at the cost of introducing a new optimization matrix P. The size of P depends on the order of G and the dynamics in Ψ, with a quadratic growth in the number of decision variables. With the aim to mitigate the computational burden associated to the study of medium-large systems, recently an alternative numerical solution of the conditions stated in Theorem 1 has been proposed.[7] Briefly, the optimization problem is solved directly using the frequency-domain inequalities (Eq. 9) starting from an arbitrary gridding. A specific algorithm, based on LFT and μ, is then applied in order to guarantee the validity of the solution on the frequency-domain continuum.
This technique, having the advantage of not relying on the (high-dimensional) optimization matrix P, is available with the SMAC toolbox[4] and will be employed in this work for the analyses.

3. Aeroelastic system

Flutter analysis studies the conditions at which the dynamic aeroelastic system loses its stability. This is a speed-dependent problem, since as the airspeed V varies then the system's behavior changes. The result is the prediction of the so-called flutter speed V_f, below which the system is guaranteed to be stable. It is therefore a prerequisite of the following analyses the availability of a model capturing the fluid structure interaction effects.

The *typical section* model was introduced in the early stages of aeroelasticity to investigate dynamic phenomena such as flutter.[5] Despite its simplicity, it captures essential effects in a simple model representation, see Fig. 4.

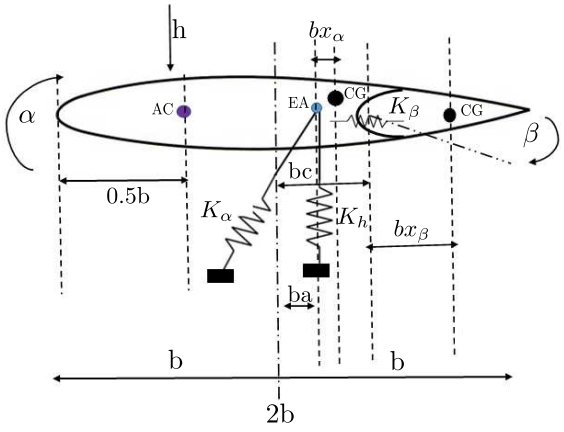

Figure 4: Typical section sketch

It consists of a rigid airfoil with lumped springs simulating the 3 degrees of freedom (DOFs): plunge h, pitch α and trailing edge flap β. The position of elastic axis (EA), center of gravity (CG) and aerodynamic center (AC) is marked in Fig. 4. The parameters in the model are: K_h, K_α and K_β –respectively the bending, torsional and control surface stiffness; half chord distance b; dimensionless distances a, c (from the mid-chord to respectively the flexural axis and the hinge location), and x_α and x_β (from flexural axis to airfoil center of gravity and from hinge location to

control surface center of gravity); wing mass per unit span m_s; moment of inertia of the section about the elastic axis I_α; and the moment of inertia of the control surface about the hinge I_β. The structural damping can be expressed specifying the damping ratios for each DOFs and then applied through modal damping approach.[6]
The Theodorsen unsteady formulation proposed in[21] is employed as aerodynamic model. This approach is based on the assumption of a thin airfoil moving with small harmonic oscillations in a potential and incompressible flow. The same hypotheses underline most of the more advanced aerodynamic approaches (e.g. Doublet Lattice Method).

In order to present the basic model development approach, $\mathbf{X}$ and $\mathbf{L_a}$ are defined as the vectors of the degrees of freedom and of the aerodynamic loads respectively:

$$\mathbf{X}(t) = \begin{bmatrix} \frac{h(t)}{b} \\ \alpha(t) \\ \beta(t) \end{bmatrix}; \quad \mathbf{L_a}(t) = \begin{bmatrix} -L(t) \\ M_\alpha(t) \\ M_\beta(t) \end{bmatrix} \tag{12}$$

The set of differential equations describing the dynamic equilibrium (Lagrange's equations)[12] can be recast in matrix form as follows:

$$[\mathbf{M_s}]\ddot{\mathbf{X}} + [\mathbf{C_s}]\dot{\mathbf{X}} + [\mathbf{K_s}]\mathbf{X} = \mathbf{L_a} \tag{13}$$

where $\mathbf{M_s}$, $\mathbf{C_s}$ and $\mathbf{K_s}$ are respectively the structural mass, damping and stiffness matrices. The expression of $\mathbf{L_a}$, provided in the Laplace s domain, is:

$$\mathbf{L_a}(s) = q[\mathbf{A}(\bar{s})]\mathbf{X}(s) \tag{14}$$

where the dynamic pressure q and the dimensionless Laplace variable $\bar{s}$ ($=s\frac{b}{V}$ with V the airspeed) are introduced. $\mathbf{A}(\bar{s})$ is called the generalized Aerodynamic Influence Coefficient (AIC) matrix, and is composed of generic terms $\mathbf{A}(\bar{s})_{ij}$ representing the transfer function from each degree of freedom j in $\mathbf{X}(s)$ to each aerodynamic load component i in $\mathbf{L_a}(s)$. Due to the motion assumptions underlying Theodorsen theory, the expression in (14) has to be evaluated at $\bar{s}=i\frac{\omega b}{V}=ik$, where k is called *reduced frequency*.
The final aeroelastic equilibrium is inherently expressed in frequency-domain and is given by:

$$\Big[[\mathbf{M_s}]s^2 + [\mathbf{C_s}]s + [\mathbf{K_s}]\Big]\mathbf{X} = q[\mathbf{A}(\bar{s})]\mathbf{X} \tag{15}$$

Using Eq. (15), for example with the *p-k* method, the objective is to find the determinant roots s such that nonzero solutions for $\mathbf{X}$ exist.[12] This is the most common approach to nominal flutter analysis since this is the framework where the aerodynamic loads are more accurately expressed for this purpose.

On the other hand, in order to express the equilibrium in state space, which is essential to deal with aeroservoelastic problems and control based techniques, a rational approximation of $\mathbf{A}(\bar{s})$ has to be performed. In this work Minimum State (MS)[15] method is employed, which enables to obtain a state-space description of the system:

$$\begin{bmatrix} \dot{\hat{\mathbf{X}}}_\mathbf{s} \\ \dot{\hat{\mathbf{X}}}_\mathbf{a} \end{bmatrix} = \hat{\mathbf{A}} = \begin{bmatrix} \hat{\mathbf{A}}_{ss} & \hat{\mathbf{A}}_{sa} \\ \hat{\mathbf{A}}_{as} & \hat{\mathbf{A}}_{aa} \end{bmatrix} \begin{bmatrix} \hat{\mathbf{X}}_\mathbf{s} \\ \hat{\mathbf{X}}_\mathbf{a} \end{bmatrix} \tag{16}$$

where $\hat{\mathbf{A}}$ is the state-matrix, $\hat{\mathbf{X}}_\mathbf{s}$ and $\hat{\mathbf{X}}_\mathbf{a}$ are respectively the structural and aerodynamic states, the latter needed for the rational approximation of the unsteady operator. The reason why MS method is chosen is that it ensures the lowest size for $\hat{\mathbf{X}}_\mathbf{a}$ compared to other approximation algorithms. The interested reader is referred to[13] for further discussions about the implementation of different aerodynamic approximations and their impact on robust flutter analysis. The total size of the plant n in this example is 9 (6 structural and 3 aerodynamic states). The nominal parameters defining the typical section studied in this work are taken from,[20] whereas an example of linear nominal flutter analysis and a comparison of the results obtained with this model and others from literature are reported in.[14]

4. A methodology for detection and analysis of Limit Cycle Oscillations

One of the main applications of DF method is the study of the existence of steady oscillations in nonlinear systems. In particular, Limit Cycle Oscillations[22] are of engineering interest, which are defined as initial condition-independent isolated periodic orbits which occurs in unforced dissipative (nonconservative) systems. It is well ascertained that the characterization of a Limit Cycle, in terms of its range of existence and approximate amplitude and frequency, is a prerequisite for good system design.[3] This Section outlines a methodology to detect LCOs and study their stability.

4.1 Detection of freeplay-induced LCOs

In Section 2.1 the basic principles of DF method were described, and in particular it was concluded that it is possible to replace the nonlinear operator with its describing function $N(A, \omega)$. Due to the well established usage of the DF method in the control community, an expression of $N(A, \omega)$ can be found for the majority of nonlinearities commonly encountered in applications.[11] As a preliminary, it is noted that the complex gain in Eq. (3) can be interpreted as an operator which acts upon a sinusoidal input and gives the phased sinusoidal output (i.e. proportional plus derivative element), or in other words:

$$N(A, \omega) = \frac{b_1 + ja_1}{A} = n_p(A, \omega) + jn_q(A, \omega) = n_p + \frac{n_q}{\omega}s \tag{17}$$

where the subscripts p and q are used to stress the in-phase and quadrature nature of the gains of the nonlinearity. An important class of nonlinearities is represented by the single-valued, or memoryless, for which n_q=0. If the nonlinearity is also static (no dependence upon the input derivatives) then n_p=$n_p(A)$, i.e. the gain does not depend on frequency.
An example of nonlinearity holding these properties is freeplay, also called dead-zone or threshold, which often arises in mechanical and electrical systems where the first part of the input is needed to overcome an initial opposition at the output, as schematically depicted in Fig. 5. Its explicit mathematical definition is given by:

$$w = \begin{cases} k(v - \bar{\delta}); & |v| > \bar{\delta} \\ 0; & |v| < \bar{\delta} \end{cases} \tag{18}$$

where $\bar{\delta}$ is defined as the (positive) freeplay size.

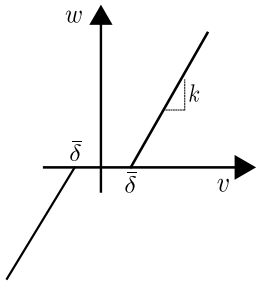

Figure 5: Freeplay nonlinearity

Recalling the aeroelastic model presented in Section 3, the freeplay nonlinearity is concentrated in the diagonal term of the stiffness matrix K_s corresponding to the control surface rotation degree of freedom. If the freeplay is schematized as in Eq. (18), the corresponding elastic moment M_β^E can be written as:

$$M_\beta^E = \begin{cases} K_\beta^L(\beta - \bar{\delta}); & |\beta| > \bar{\delta} \\ 0; & |\beta| < \bar{\delta} \end{cases} \tag{19}$$

where K_β^L is the flap stiffness in the linear case.
The DF function N^F associated to freeplay can be obtained analytically[11] by applying the definition in Eq. (3):

$$N^F(\beta_s) = \begin{cases} 0; & \beta_s < \bar{\delta} \\ \frac{k}{\pi}\left[\pi - 2\sin^{-1}(\frac{\bar{\delta}}{\beta_s}) - 2(\frac{\bar{\delta}}{\beta_s})\sqrt{1 - (\frac{\bar{\delta}}{\beta_s})^2}\right]; & \beta_s > \bar{\delta} \end{cases} \tag{20}$$

where β_s is the amplitude of the harmonic motion of the control surface. Due to the aforementioned properties held by this nonlinearity, its describing function (depicted in Fig. 6) is a pure real gain not depending on frequency, but only on the amplitude of the input signal A (here specified as β_s), in particular on its ratio with $\bar{\delta}$.
The application of DF enables finally to give an expression for the elastic moment M_β^E in (19) as:

$$\begin{aligned} M_\beta^E &= K_\beta^{QL}(\beta_s)\beta \\ K_\beta^{QL}(\beta_s) &= N^F(\beta_s)K_\beta^L \end{aligned} \tag{21}$$

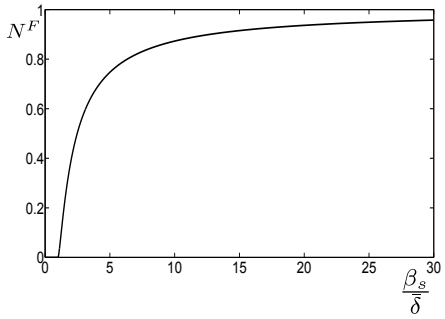

Figure 6: Freeplay Describing Function

where $K_\beta^{QL}(\beta_s)$ is the quasi-linear flap stiffness and $N^F(\beta_s)$ is taken from (20) with $k = 1$ (note that $0 < N^F < 1$). In other words, the nonlinear flap stiffness K_β is replaced by the quasi-linear stiffness $K_\beta^{QL}(\beta_s)$, which is a function of the flap rotation amplitude β_s.

The methodology employed to study LCOs through DF takes the clue from the feedback representation of a nonlinear system in Fig. 1, specialised by specifying the signal circulating through the system as a sinusoid, and replacing the nonlinear element by its describing function N^F. Linear theory is then applied to the quasi-linearized system, searching for points of neutral stability which are interpreted as LCOs in the original (nonlinear) system. The well-known feedback relations involve the frequency response of the signals (in capital letters) and the transfer functions of the operators, and the resulting necessary condition for oscillations are:

$$\begin{aligned} V(j\omega) &= -G(j\omega)W(j\omega) \\ W(j\omega) &= N^F(\beta_s)V(j\omega) \\ [1 + G(j\omega)N^F(\beta_s)]V(j\omega) &= 0 \end{aligned} \tag{22}$$

Solution of the characteristic equation gives the conditions in terms of β_s and ω such that the system exhibits self-sustained oscillations, i.e. amplitude and frequency of the LCO are determined. Both algebraic and graphical methods can be employed in order to solve Eq. (22). In the former case, a numerical solution is often required since the DF expression does not allow an analytical formulation of the roots of the loop transfer function (recall for example Eq. 20). The solution through graphical methods closely resembles the rationale of Nyquist and Nichols plot.[10] Typically the characteristic equation is rewritten as follows:

$$G(j\omega) = -\frac{1}{N^F(\beta_s)} \tag{23}$$

Both sides of Eq. (23) are plotted in the complex plane and the intersection points of the curves are found. Since N^F does not depend on the frequency, i.e. the left-hand side curve is parameterized with ω while the right-hand side with β_s, all the intersections correspond to LCOs and directly provide amplitude and frequency of the oscillation.

4.2 Stability of the LCOs

The characteristic equation in Eq. (22) gives only a necessary condition for the occurrence of periodic oscillations in the nonlinear system. Even if the DF hypotheses are all satisfied, stability of the oscillation has still to be verified.[22] The question of LCO stability is generally posed in terms of the states trajectory behavior following amplitude or frequency perturbations. If the LCO returns to its original equilibrium state it is defined *stable*, whereas if its amplitude or frequency change in order to reach another equilibrium state, it is defined *unstable*.
To tackle the stability problem algebraically, the methodology proposed in[1] is here adopted. The complex eigenvalue associated to the LCO is named λ_{LC}=σ+jω, with σ=0 when the necessary condition for oscillations is satisfied. The idea is to study the variation of the real part σ following a perturbation in the LCO amplitude β_s. The general spectral decomposition allows to express the state-matrix $\hat{\mathbf{A}}$ as:

$$\hat{\mathbf{A}} = \sum_{k=1}^{\hat{N}} \lambda_k \mathbf{u}_k \mathbf{v}_k^T \tag{24}$$

where $\mathbf{u}_k$ and $\mathbf{v}_k$ are the right and left eigenvectors corresponding to the eigenvalue λ_k and $\hat{N}$ is the size of $\hat{\mathbf{A}}$. Starting from Eq. (24) and taking advantage of the orthogonal property of left and right eigenvectors, the following holds:[1]

$$\frac{\partial \sigma}{\partial \beta_s} = \mathrm{Re}\left(\mathbf{v}_{LC}^T \frac{\partial \hat{\mathbf{A}}}{\partial \beta_s} \mathbf{u}_{LC}\right) \tag{25}$$

By means of the relation in Eq. (21), it is possible to express the nonlinear term in the state-matrix as a function of the control surface oscillation amplitude β_s and thus analytically perform the derivative. A stable limit cycle requires $\frac{\partial \sigma}{\partial \beta_s} < 0$, since a positive perturbation in amplitude moves the trajectory outside the limit cycle and requires a decay in the amplitude (negative real part) to move the trajectory back to the limit cycle, and conversely an unstable limit cycle will have $\frac{\partial \sigma}{\partial \beta_s} > 0$.

The application of this procedure is limited to systems described in state-space form. However, as highlighted in Section 3, for flutter analysis applications the aeroelastic system is typically described and studied in the frequency-domain. It is therefore desirable to find for this latter representation an equivalent condition of Eq. (25).
For this purpose, let us define $\bar{\mathbf{B}}(j\omega)$ the frequency response matrix of the aeroelastic system defined in Eq. (15):

$$\bar{\mathbf{B}}(j\omega) = [\mathbf{M_s}]s^2 + [\mathbf{C_s}]s + [\mathbf{K_s}] - q[\mathbf{A}(\bar{s})] \tag{26}$$

and its total derivative with respect to the LCO amplitude as:

$$\frac{\partial \bar{\mathbf{B}}}{\partial \beta_s} = \frac{\partial \bar{\mathbf{B}}}{\partial s}\frac{\partial s}{\partial \beta_s} + \frac{d\bar{\mathbf{B}}}{d\beta_s} \tag{27}$$

Eq. (27) features the term $\frac{\partial s}{\partial \beta_s}$, which describes the variation of the considered eigenvalue when perturbing the LCO amplitude and thus it is sought here to address the study of LCO stability in frequency-domain.
Let us note that the roots s_k found by the *p-k* method (i.e. fulfilling Eq. (15) for the non-trivial case $\mathbf{X} \neq \mathbf{0}$), are such that:

$$[\bar{\mathbf{B}}(s_k)]\mathbf{X} = \mathbf{0} \quad \equiv \quad [\bar{\mathbf{A}} - s_k\mathbf{I}]\mathbf{X} = \mathbf{0} \tag{28}$$

where $\bar{\mathbf{A}}$ is implicitly defined by Eq. (28) and represents an *equivalent* state-matrix in that, having defined $\mathbf{U}_k$ and $\mathbf{V}_k$ as its right and left eigenvectors corresponding to the eigenvalue s_k, the following property holds:

$$\mathbf{V}_k^T \bar{\mathbf{B}} \mathbf{U}_k = \mathbf{0} \tag{29}$$

As a result of Eq. (29), and of known properties of eigenvectors, the following relation is finally obtained:

$$\frac{\partial(\mathbf{V}_k^T \bar{\mathbf{B}} \mathbf{U}_k)}{\partial \beta_s} = \frac{\partial \mathbf{V}_k^T}{\partial \beta_s}\bar{\mathbf{B}}\mathbf{U}_k + \mathbf{V}_k^T \frac{\partial \bar{\mathbf{B}}}{\partial \beta_s}\mathbf{U}_k + \mathbf{V}_k^T \bar{\mathbf{B}}\frac{\partial \mathbf{U}_k}{\partial \beta_s} = \mathbf{V}_k^T \frac{\partial \bar{\mathbf{B}}}{\partial \beta_s}\mathbf{U}_k = 0 \tag{30}$$

Eq. (30) is key because it enables to explicitly express the derivative of the root s associated to the LCO condition. By substituting Eq. (27) in Eq. (30), it is finally obtained:

$$\frac{\partial s_k}{\partial \beta_s} = -\frac{\mathbf{V}_k^T \frac{d\bar{\mathbf{B}}}{d\beta_s}\mathbf{U}_k}{\mathbf{V}_k^T \frac{\partial \bar{\mathbf{B}}}{\partial s}\mathbf{U}_k} \tag{31}$$

Eq. (31) provides the variation of the generic root s_k when the LCO amplitude is perturbed. By evaluating its real part at the LCO condition, an equivalent criterion as the one in Eq. (25) is obtained:

$$\mathrm{Re}\left(\frac{\partial s_k}{\partial \beta_s}\right)\Big|_{k=LC} = -\,\mathrm{Re}\left(\frac{\mathbf{V}_{LC}^T \frac{d\bar{\mathbf{B}}(s_{LC})}{d\beta_s}\mathbf{U}_{LC}}{\mathbf{V}_{LC}^T \left.\frac{\partial \bar{\mathbf{B}}(s_k)}{\partial s_k}\right|_{LC}\mathbf{U}_{LC}}\right) \tag{32}$$

The calculation of the partial derivatives in Eq. (32) can be performed recalling the definition of $\bar{\mathbf{B}}$ in Eq. (26):

$$\begin{aligned} \left.\frac{d\bar{\mathbf{B}}}{d\beta_s}\right|_{LC} &= \frac{d\mathbf{K_s}(\beta_s)}{d\beta_s} \\ \left.\frac{\partial \bar{\mathbf{B}}}{\partial s}\right|_{LC} &= 2\mathbf{M_s}s_{LC} + \mathbf{C_s} - \frac{d\mathbf{A}(\bar{s})}{ds} \end{aligned} \tag{33}$$

The first expression can be straightforwardly evaluated once the relation in Eq. (21) is substituted in $\mathbf{K_s}$, whereas the latter equation features $\frac{d\mathbf{A}}{ds}$. Recalling that the AIC matrix only depends on the imaginary part of s, it holds that

$\frac{d\mathbf{A}}{ds} = \frac{d\mathbf{A}}{d\omega}$. This can be evaluated by means of a finite difference scheme or employing a rational approximation for the aerodynamic operator. It is the authors' opinion, however, that this term is negligible compared to the others two in the expression of $\frac{\partial \mathbf{B}}{\partial s}$. This assessment was quantitatively verified on this test case, and it is qualitatively supported by the fact that in the flutter range the aerodynamic operator has typically a smooth variation with respect to the frequency[13] .

Finally, graphical methods for the study of LCO stability are based on the same rationale. Once the framework for graphical LCOs detection is employed and thus the intersections given by Eq.23 are depicted in the complex plane, the Nyquist theorem can be used. Again, it is sought how the quasi-linearized system will behave in response to the perturbation in oscillation amplitude, whether settling back to the original value or moving towards a different equilibrium. This is done by checking the encirclements around the new location of the critical point and applying the well-known Nyquist theorem for linear stability. An example will be provided in Section 5.2.

5. Application to the aeroelastic nonlinear benchmark

The aeronautical industry has sensibly strengthen his focus on nonlinear phenomena in the last decade[8] and thus increasing effort has been devoted on this topic by the research community. An example of this effort is the benchmark study of an airfoil affected by control surface freeplay.[6,20] This Section shows the results of the analyses applied to this test case when the system parameters are nominal and when they are affected by uncertainties. In the former case, both algebraic and graphical results are proposed, whereas in the latter case μ analysis is used in conjunction with DF. Finally, a validation of the analyses by means of IQC is discussed.

5.1 Algebraic analysis

The procedure to detect necessary conditions for LCOs in the plant, building on the methodology outlined in Section 4.1, is here applied to the analyzed test case. A fundamental harmonic solution for the flap rotation β=$\beta_s \sin(\omega t)$ is assumed and from Eq. (20) the corresponding value of N^F is obtained. This enables to calculate the quasi-linear stiffness K_β^{QL} (Eq. 21) and thus evaluate the corresponding flutter speed V_f, defined as the lowest speed which drives the system unstable, and the corresponding flutter frequency ω_f.
Fig. 7 showcases the values of flutter speed V_f and associated frequency ω_s (in this case evaluated through eigenvalue analysis of Eq. (16), i.e. the state-space approach) corresponding to a variation of flap stiffness between 0 and the linear value $K_\beta^L = 3.9N$. An interesting feature detectable in Fig. 7 is the existence, depending on the value of K_β^{QL}, of a low (LF) and high (HF) flutter frequency (dashed line) associated to the instability. The physical reason for this is that two different modes, respectively the plunge and pitch one, go unstable (i.e. are associated to the smallest unstable speed V_f) as K_β^{QL} varies. The results are in good agreement with those from the literature[6,20] (the latter reference provides also experimental results).

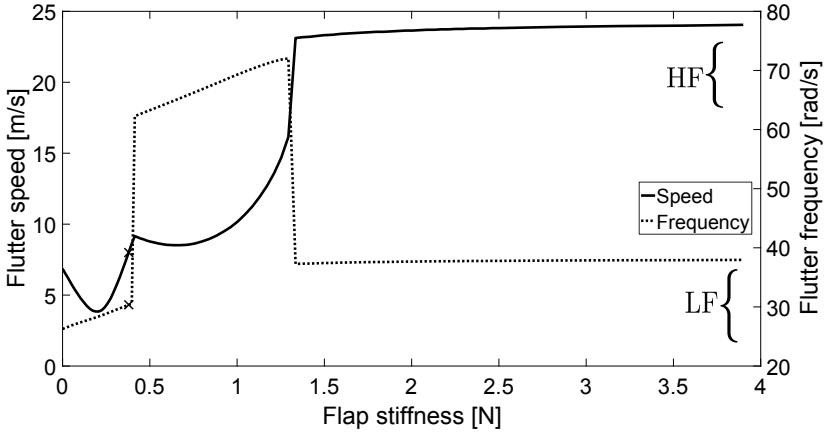

Figure 7: Flutter speed (left y-axis) and frequency (right y-axis) vs. quasi-linear flap stiffness K_β^{QL}

The DF method enables to infer conclusions about the nonlinear response of the system due to the freeplay, namely amplitude, frequency and stability of LCOs. In particular, the conditions of neutral stability for the quasi-linearized system (reported in Fig. 7) are associated to LCOs in the nonlinear system. The DF method is instrumental in guaranteeing the connection between these two representations and enabling to transfer the information coming from multiple linear flutter analyses to LCO characterization. In Fig. 8 the nondimensional flap rotation LCO amplitude $\frac{\beta_s}{\delta}$ is plotted

against airspeed. In order to validate the methodology proposed in Section 4.2 to detect stable and unstable oscillations when the plant is described in frequency-domain, two curves are shown: the one labelled with *SS* (black curve) build on the flutter speeds found with the eigenvalue analysis of the state-matrix in Eq. (16) and the criterion used is thus the one in Eq. (25), whereas *FD* (red cruve) is derived from an in-house implementation of the *p-k* method (which solves Eq. 15) and the criterion used is the one proposed in this paper (Eq. 31). The two curves are in good agreement (indeed almost indistinguishable), and most importantly the same ranges of stable (solid line) and unstable (dashed line) oscillations are detected, therefore validating the proposed approach.

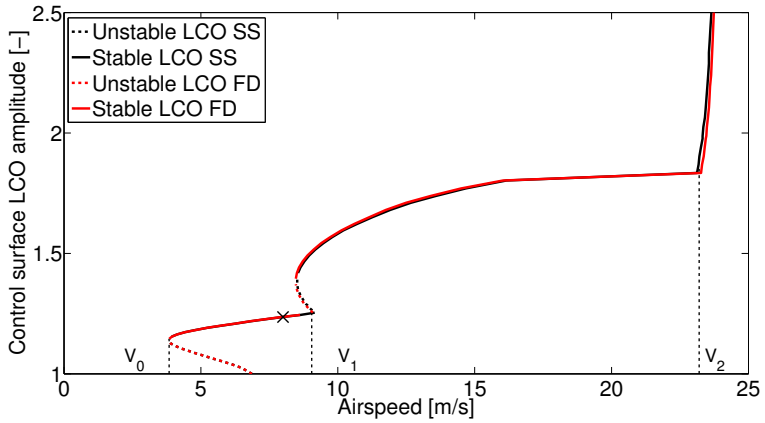

Figure 8: Flap rotation LCO amplitude $\frac{\beta_s}{\delta}$ vs. airspeed V

Four regions can be identified in Fig. 8 as the airspeed increases: (i) $V<V_0(=3.8\frac{m}{s})$, where the system is stable; (ii) $V_0<V<V_1(=9\frac{m}{s})$, where the system undergoes LCOs associated with the plunge instability (with amplitude given by the upper stable branch); (iii) $V_1<V<V_2(=23.2\frac{m}{s})$ where the LCO switches to the pitch instability (the frequency correspondingly changes, as in Fig. 7) and the amplitude visibly increases; and (iv), for speeds greater than V_2 where there is an asymptote in the LCO amplitude corresponding to a dramatic growth of the airfoil oscillations. It is worth noting that the maximum speed for which the system does not experience LCO (i.e. V_0) is considerably smaller than the flutter speed evaluated with a linear model (identified in Fig. 7 for $K_\beta^{QL} = K_\beta^L$).

5.2 Graphical analysis

In this section the nonlinear analysis of the test case is performed adopting a graphical approach. The problem is rearranged to fit to the LFT framework. To this end, the system is divided into the linear (known) part G (describing the system with zero freeplay) and a block named $\hat{\Phi}$ which holds the nonlinearity. This feedback configuration, representing a connection between standard DF (Fig. 1) and LFT (Fig. 2) representations, is depicted in Fig. 9.

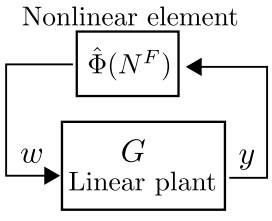

Figure 9: LFT representation of the DF quasi-linearized system for graphical LCO study

The $\hat{\Phi}$ block is thus defined such that, when the linear case is recovered (i.e. N^F=1), it gives zero output:

$$\hat{\Phi}(N^F) = -K_\beta^L(1 - N^F(\beta_s)) \tag{34}$$

$\hat{\Phi}$ varies from 0 to $-K_\beta^L$ (equivalently, $N^F(\beta_s) \in [0,1]$ as in Fig. 6) and its effect is to decrease the flap stiffness of the system depending on the value of β_s.
The necessary condition for the occurrence of LCOs is then (note that there is a *minus* sign due to the positive feedback of the LFT):

$$1 - G(j\omega)\hat{\Phi}(N^F) = 0 \tag{35}$$

Since $\hat{\Phi}(N^F)$ is here a real scalar, it suffices to find the intersections of $G(j\omega)$ with the real axis. For ease of representation and calculation, $\hat{\Phi}$ and G are scaled such that the former is normalized (i.e. $G \in$ [-1,1]). Then, once a speed V is selected, the calculation can be performed. In Fig. 10 the process is exemplified by depicting $G(j\omega)$ for the case V=8$\frac{m}{s}$.

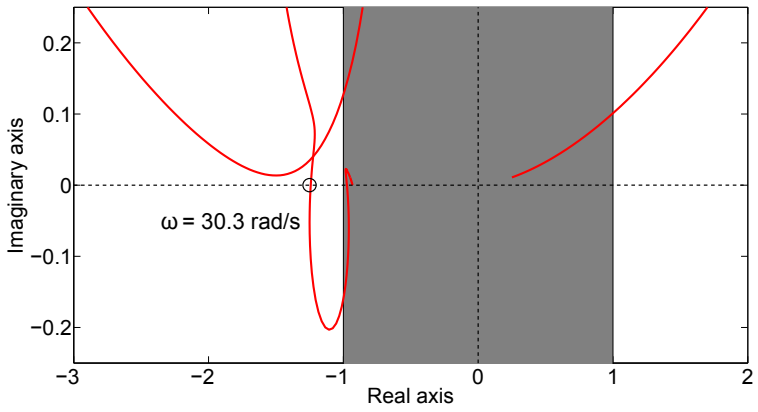

Figure 10: Graphical study of LCOs necessary condition at V=8$\frac{m}{s}$

From Eq. (35) it follows that the intersections of G with the real axis represent values of $\hat{\Phi}$ associated with possible LCOs. At the intersections it holds indeed:

$$\hat{\Phi}(N^F) = \frac{1}{G(j\omega)} \tag{36}$$

which gives the values of N^F and ω, i.e. amplitude and frequency of the LCO. Due to the normalization, only the intersections with absolute value greater than 1 (i.e. beyond the grey area) are considered, since they correspond to absolute values of $\hat{\Phi}$ smaller than one. For this case study, 3 intersections can be spotted, with only one in the allowed range (black circled) corresponding to $G(j\ 30.3\frac{rad}{s}) = -1.25$. From these values and the relation in Eq. (36), it is possible to estimate the associated N^F and thus the corresponding flap amplitude and stiffness. It can be verified that this intersection coincides with the point highlighted in Fig. 7 with the cross marker.
This framework can be used also to study the stability of the detected LCOs. The Nyquist criterion is employed for this investigation. As the LCO amplitude is perturbed, the critical point is moved and the number of clockwise encirclements are counted. Recalling the discussion in Section 4.2, if the amplitude is increased, the change of position has to result in a stable state in order for the LCO to be stable. Focusing on the left side of Fig. 10 (where the intersection lies), it is noted that an increase in amplitude β_s (i.e. an increase in N^F) leads to an increase in $\Phi(N^F)$ and thus a decrease in the value of the critical point, i.e. the point moves towards the left.
The LCO determined graphically in Fig. 10 is therefore stable since, when the amplitude is increased then the point has zero clockwise encirclements (i.e. the quasi-linear system is stable) and thus the amplitude decays to the original value, whereas when the amplitude is decreased (i.e. point moved towards right) then the system features one clockwise encirclement, and as a consequence the amplitude is increased until the original value is reached. These conclusions are consistent with the stability analysis reported in Fig. 8 (where a cross marker was used to define the considered LCO point).

5.3 Analysis with uncertainties

A practical interpretation of the plot in Fig. 8 is that at a given airspeed V the system might experience periodic oscillations as described by the stable curve. In particular, the oscillation amplitude $\frac{\beta_s}{\delta}$ can be directly read in the y-axis. It is therefore of interest to investigate how the LCO curve varies in the face of uncertainties in the plant. The proposed approach is here summarized.
Parametric uncertainties are used to describe parameters whose values are not known with a satisfactory level of confidence. Considering a generic uncertain parameter d, with γ_d indicating the uncertainty level with respect to a nominal value d_0, a general uncertain representation is given by:

$$d = d_0 + \gamma_d \delta_d \tag{37}$$

where $\|\delta_d\| \leq 1$ to conform with the scaling in Eq. (6). This study will take into account a 10% uncertainty in the following parameters: bending stiffness K_h; torsional stiffness K_α; static moment of the aileron S_α (i.e. $S_\alpha = bx_\alpha$); the

moment of inertia of the section I_α; the moment of inertia of the control surface I_β. The selection of these parameters and of their uncertainty ranges defines the uncertainty set $\mathbf{\Delta_u}$ corresponding to the LFT representation from Eq. (4).
If an operating point in Fig. 8 (identified by the pair $\{V, \frac{\beta_s}{\delta}\}$) lying outside the region defined by the LCO curve is considered, the robust analysis performed with μ will allow to estimate how close it is to become a Limit Cycle when uncertainties are considered. In other words, the μ analysis will provide a guaranteed minimum distance to the LCO curve by evaluating a robust stability margin of the associated plant in the quasi-linearized system.
In Fig. 11 it is proposed a representation of the robust analysis results tailored for LCO studies.

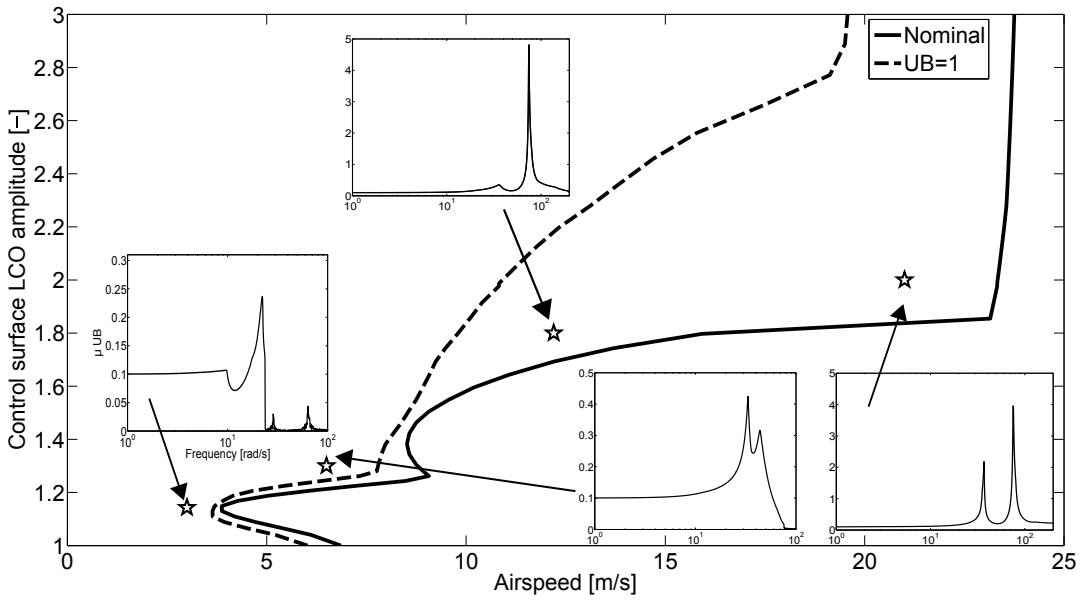

Figure 11: Robust assessment of the LCO graph for the typical section freeplay nonlinearity

The solid curve is the same LCO graph presented in Fig. 8, and the star markers represent four operating points where μ analysis is applied (the corresponding upper bounds μ_{UB} are shown in the smaller plots). As aforementioned when $\mu < 1$ then it can be inferred that the LCO curve lies below that point despite the uncertainties, that is, the worst-case amplitude of the LCO is smaller than the one associated to the operating point. Conversely, when $\mu > 1$ then the LCO curve might fall above the point for an adverse (but within the considered range) combination of parameters, meaning in practice that the oscillatory response will feature greater amplitude than the one related to that point.
These results predict the robustness of the LCO at discrete points. To provide an assessment on the overall LCO graph, a flap stiffness gridding is considered and, at each point, a bisection-like algorithm searching for the airspeed V which attains first the RS violation condition (here interpreted as $\mu_{UB} = 1$) is implemented and the resulting curve is plotted as a dashed line in Fig. 11. It is worth noting that, as expected, the two points yielding to $\mu_{UB} < 1$ (i.e. the two left most points) lie above the dashed curve, whereas the two points resulting in $\mu_{UB} > 1$ are located below it.
The stability analysis of the LCO curve obtained with the strategy outlined in this section is not reported here due to space limitations. However, once the worst-case perturbation identified by the analysis are substituted in the LFT to obtain the perturbed plant, the methodologies (either algebraic or graphic) presented in Section 4.2 can be applied.

5.4 IQC validation

Section 2.1 summarized the main hypotheses related to the application of the DF method. In particular, the assumption that the linear part of the system acts as a low pass filter (Eq. 2) is often regarded as critical for a successful application of this method. Its validity for the considered test case is thoroughly addressed in reference[17] . In this reference the Harmonic Balance, a refinement of DF method where also higher harmonics can be retained, is employed. Two cases are studied, considering respectively 1 or 3 harmonics, and overall it was concluded[6,20] that DF represents a valid tool of analysis for this particular problem.
When uncertainties are also considered in the model, additional hypotheses are involved. For example, due to the NP-hard nature of the problem, the algorithms used to evaluate μ typically rely on a frequency gridding, loosing the guarantee on the frequency continuum. In the analysis of flexible systems, prone to have sharp peaks in the μ plot, this has been highlighted as a potential source of inaccuracy[9] .
It is therefore envisaged the necessity to bolster the predictions obtained with the DF-μ approach outlined so far in this

paper, especially when applied to a generic nonlinear robust problem for which there are not results in literature. A possible strategy to address this task is represented by IQC, which is able to handle uncertainties and nonlinearities in the same framework and provide sufficient conditions for the stability of the system. As commented in the introduction to this technique in Section 2.3, the core effort is to find suitable multipliers Π_i (Eq. 8) describing the input/output relation of the operator $\mathbf{\Delta}$, since most of the conservatism associated to the results lies there. The toolbox employed for the analyses[4,7] allows to define for the nonlinear channel two static multipliers: the sector and the Popov multipliers. They are both applicable to this test case because they reflect properties held by the freeplay (Eq. 19). The former expresses the property that the output of the nonlinear element is bounded within the range $[\alpha, \eta]$ and a common choice is to specify $\alpha = 0$ and $\eta = K_\beta^L$, whereas the latter enforces the time invariance.
As for the uncertainties, the multiplier is parameterized assuming as basis functions combinations of first order low-pass filters, whose poles are specified by the user.
The methodology employed here to check the stability of the system consists in increasing the airspeed V until the IQC problem becomes unfeasible (the first airspeed for which this happens is named V_{unf}). This means that the interconnection of G and Δ in Fig. 3 cannot be proved to be *well-posed*, that is absolute stability cannot be guaranteed, with *that* particular test. In fact, it is well-known that an unfeasible IQC can also result from other issues, as for example improper choice of poles/ranges, numerical issues, too large dimension of the problem, and therefore by performing incremental tests (e.g. changing the multipliers parametrization) it is usually possible to assess that this is not the case. The analysis for the case with only freeplay and for the case with both nonlinearity and uncertainties (in this latter case the number of filters employed in the dynamic multiplier parametrization is also reported) is shown in Tab. 1.

Table 1: IQC analysis of the system

	N of poles	$V_{unf}[\frac{m}{s}]$
Nonlinear	-	3.8
Nonlinear robust	1	-
Nonlinear robust	2	3.5
Nonlinear robust	3	3.6

The V_{unf} found from the nonlinear analysis is the same as the airspeed V_0 detected in Fig. 8. The reason for this is that by choice of the bounds $[\alpha, \eta]$ as the entire sector $[0, K_\beta^L]$, only the smallest airspeed at which the system does not experience *any* unstable response can be inferred from the results. From a DF perspective, the approach of considering the entire sector is therefore equivalent to look for the smallest airspeed such that the system experiences an LCO. Similar conclusions can be drawn for the analysis with nonlinearity and uncertainties. If the number of poles used in the parametrization is increased adequately, the largest LCO-free speed in Fig. 11 is retrieved (dashed curve). Due to the good agreement in both cases, these analyses may then be seen as a validation of the application of DF to this particular test case, at least for what concerns the smallest LCO speed.
It might appear a limitation of this method the possibility to detect *only* the largest speed for which the system is absolute stable, as it would be desirable to obtain further information. For example, while IQC analysis detects a small influence of the uncertainties in modifying the smallest LCO speed, the provided results do not capture the remarkable growth in amplitude clearly spotted in Fig. 11 for higher speeds. The reason for this is that with the standard definition of the nonlinear sector, the certificates found guarantee *global* stability of the system, at the cost of high conservatism. It will be the focus of future work the study of different sector bound constraints such that *local* certificates can be obtained. On the one hand, this would have the advantage of providing less conservative stability guarantees for the system, and on the other it would enable IQC to validate the results coming from the DF-μ approach to a larger extent.

6. Conclusions

This work investigates a possible methodology to study the stability properties of an aeroelastic system subject to freeplay nonlinearity and LTI parametric uncertainties.
The proposed approach consists of the joint use of the Describing Functions method (to model nonlinearities) and of the μ analysis method (to predict the stability of the system). After introducing the techniques and the aeroelastic model employed, a systematic approach is presented, which enables to study both algebraically and graphically the problem of detecting LCOs and study their stability. In this regard, the paper proposes an algorithm to evaluate whether the detected oscillations are stable or not when the aeroelastic plant is formulated in frequency-domain.
The application of the DF-μ framework to an aeroelastic benchmark is presented, showing the potentialities in characterizing the nonlinear response of the system in terms of airspeed range, approximate amplitude and frequency quantification, both in the case of nominal and uncertain systems. The proposed validation with IQC confirms that the largest speed for which the system is LCO free is well captured, but no further information is available due to the global nature of IQC analysis. Future work will explore less conservative (i.e. local) predictions.

References

[1] M.R. Anderson. Pilot-induced oscillations involving multiple nonlinearities. *J. of Guidance, Control and Dynamics*, Vol. 21(5):pp. 786–791, 1998.

[2] G.J. Balas, R. Chiang, A. Packard, and M. Safonov. *Robust Control Toolbox*. 2009.

[3] P. Bansal and D.M. Pitt. Uncertainties in control surface free-play and structural properties and their effect on flutter and LCO. AIAA Scitech Conference, January 2014.

[4] J-M. Biannic, L. Burlion, F. Demourant, G. Ferreres, G. Hardier, T. Loquen, and C. Roos. The SMAC Toolbox: a collection of libraries for Systems Modeling, Analysis and Control, available at http://w3.onera.fr/smac/.

[5] R. L. Bisplinghoff and H. Ashley. *Principles of Aeroelasticity*. Wiley, New York, 1962.

[6] M.D. Conner, D.M. Tang, E.H. Dowell, and L.N. Virgin. Nonlinear Behavior of a Typical Airfoil Section with Control Surface Freeplay. A Numerical and Experimental Study. *Journal of Fluids and Structures*, 11(1):89 – 109, 1997.

[7] F. Demourant. New algorithmic approach based on integral quadratic constraints for stability analysis of high order models. European Control Conference, July 2013.

[8] E. Dowell, J. Edwards, and T. Strganac. Nonlinear aeroelasticity. *Journal of Aircraft*, Vol. 40(5), 2003.

[9] G. Ferreres. *A practical approach to robustness analysis with aeronautical applications*. Kluwer Academic, New York, 1999.

[10] C. Fielding and P.K. Flux. Non-linearities in flight control systems. *The Aeronautical Journal*, 107(1077):673–686, 2003.

[11] A. Gelb and W. E. Vander Velde. *Multiple-Input Describing Functions and Nonlinear System Design*. McGraw-Hill, 1968.

[12] D. H Hodges and G A. Pierce. *Introduction to Structural Dynamics and Aeroelasticity*. Cambridge University Press, 2011.

[13] A. Iannelli, A. Marcos, and M. Lowenberg. Aeroelastic modeling and stability analysis: a robust approach to the flutter problem. *International Journal of Robust and Nonlinear Control (accepted)*, 2017.

[14] A. Iannelli, A. Marcos, and M. Lowenberg. Limit Cycle Oscillation amplitude tailoring based on Describing Functions and μ Analysis. In *Advances in Aerospace Guidance, Navigation and Control*, 2017.

[15] M. Karpel. Design for Active and Passive Flutter Suppression and Gust alleviation. Technical Report 3482, NASA, 1981.

[16] R Lind and M Brenner. Flutterometer: An on-line tool to predict robust flutter margins. *Journal of Aircraft*, Vol. 37(No. 6), 2000.

[17] Liu, L. and Dowell, E. H. Harmonic Balance Approach for an Airfoil with a Freeplay Control Surface. *AIAA Journal*, 43(4):802–815, April 2005.

[18] A. Megretski and A. Rantzer. System analysis via integral quadratic constraints. *IEEE Transactions on Automatic Control*, 42(6):819–830, Jun 1997.

[19] Chris L. Pettit. Uncertainty Quantification in Aeroelasticity: Recent Results and Research Challenges. *Journal of Aircraft*, 41(5):1217–1229, 2004.

[20] D. Tang, E.H. Dowell, and L.N. Virgin. Limit Cycle Behavior of an Airfoil with a Control Surface. *Journal of Fluids and Structures*, 12(7):839 – 858, 1998.

[21] T. Theodorsen. General Theory of Aerodynamic Instability and the Mechanism of flutter. Technical Report 496, Naca, 1935.

[22] P. Wiggins. *Introduction to Applied Nonlinear Dynamical Systems and Chaos*. Springer-Verlag New York, 2003.

[23] K. Zhou, J. C. Doyle, and K. Glover. *Robust and Optimal Control*. Prentice-Hall, Inc., Upper Saddle River, NJ, USA, 1996.